

Robust Bayesian Functional Principal Component Analysis

Jiarui Zhang

Department of Statistics and Actuarial Science, Simon Fraser University

Jiguo Cao

Department of Statistics and Actuarial Science, Simon Fraser University

Liangliang Wang

Department of Statistics and Actuarial Science, Simon Fraser University

July 20, 2023

Abstract

We develop a robust Bayesian functional principal component analysis (FPCA) by incorporating skew elliptical classes of distributions. The proposed method effectively captures the primary source of variation among curves, even when abnormal observations contaminate the data. We model the observations using skew elliptical distributions by introducing skewness with transformation and conditioning into the multivariate elliptical symmetric distribution. To recast the covariance function, we employ an approximate spectral decomposition. We discuss the selection of prior specifications and provide detailed information on posterior inference, including the forms of the full conditional distributions, choices of hyperparameters, and model selection strategies. Furthermore, we extend our model to accommodate sparse functional data with only a few observations per curve, thereby creating a more general Bayesian framework for FPCA. To assess the performance of our proposed model, we conduct simulation studies comparing it to well-known frequentist methods and conventional Bayesian methods. The results demonstrate that our method outperforms existing approaches in the presence of outliers and performs competitively in outlier-free datasets. Furthermore, we illustrate the effectiveness of our method by applying it to environmental and biological data to identify outlying functional data. The implementation of our proposed method and applications are available at <https://github.com/SFU-Stat-ML/RBFPCA>.

Keywords: Functional data analysis, Robust estimation, Sparse functional data, Multivariate skew elliptical distribution, Outlier detection

1 Introduction

The development of modern technology has resulted in the continuous recording of data during a given period in many scientific fields, such as neuroscience, biology, and environmental science. These data can be categorized as functional data (Ramsay and Silverman, 2005b; Ferraty and Vieu, 2006; Horváth and Kokoszka, 2012; Hsing and Eubank, 2015), which are usually observed over time, space or any other continuous domain. For instance, Figure 1 displays two examples of functional data. Figure 1a shows a collection of densely observed trajectories from the Hawaii Ocean Oxygen dataset, wherein certain outlying trajectories have been highlighted. Figure 1b presents one illustration of sparse function data from the CD4 dataset, with only a few observations per curve. Both datasets have a few curves demonstrating unusual patterns in contrast to the rest.

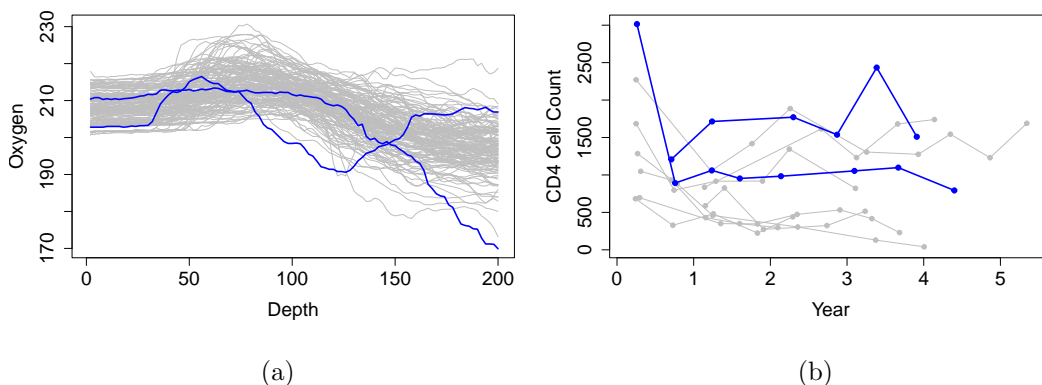


Figure 1: (a) Hawaii Ocean Oxygen data contains 133 densely observed trajectories for oxygen concentrations measuring at different depths below the sea surface. The two blue trajectories exhibit atypical behaviors in comparison with the remaining ones. (b) A subset of CD4 data with 10 sparsely observed trajectories for CD4 cell counts are shown to demonstrate the sparse nature. The two trajectories colored in blue display abnormal patterns.

As the number of functional data can grow rapidly, data compression is vital for functional data. Functional principal component analysis (FPCA) plays a crucial role in functional data analysis (FDA) as a dimension reduction technique. FPCA can be viewed as

an exploratory analysis tool to discover the hidden structure of the data by capturing the optimal low-dimensional representation and the major source of variations among curves. FPCA can also be used to help reconstruct partially-observed functions or used as a pre-processing step for regression analysis (Reiss et al., 2017) or clustering tasks (Margaritella et al., 2021). The frequentist analysis of FPCA is a mature field. Numerous works have been proposed to explore fully or densely observed function data (Dauxois et al., 1982; Rice and Silverman, 1991; Cardot, 2000; Hall and Hosseini-Nasab, 2006). Studies of the FPCA approach for sparsely observed data, a more challenging situation, can also be seen in James et al. (2000), Yao et al. (2005), and Paul and Peng (2009). Wang et al. (2016) provided a detailed review of methods, open questions and applications of FPCA.

In contrast, there has been limited investigation into the Bayesian viewpoint of FPCA. The lack of Bayesian methodologies in FDA and FPCA may be due to the challenges involved in specifying the full probability model and the limited availability of inferential tools for implementation. Nonetheless, the Bayesian framework is appealing from at least three perspectives. First, the Bayesian methods are capable of quantifying uncertainty in a straightforward manner, such as through credible intervals. Second, the Bayesian inferential structure is flexible as it can incorporate subject matter expertise in the definition of prior structures. Last but not least, the Bayesian framework also provides a straightforward approach for conducting model selection by marginal likelihood estimates.

One example of applying Bayesian methodologies in FPCA is presented by Behseta et al. (2005), who utilize a hierarchical Gaussian process model to assess variability among functions. Later, Van Der Linde (2008) proposed analyzing the modes of variation of curves via variational inference. The prevalent strategy has been to work within the hierarchical representation of the FPCA model and specify the prior distributions for all model parameters (Crainiceanu and Goldsmith, 2010; Margaritella et al., 2021). Alternatively, Suarez and Ghosal (2017) proposed a Bayesian FPCA method using approximate spectral decomposition and modelled the number of principal components with truncated Poisson distributions. For partially observed functional data, Jiang et al. (2020) considered a Bayesian model for sparse FPCA using a reduced rank mixed-effects framework. To

the best of our knowledge, no existing literature has explored outlier detection within the context of a robust Bayesian FPCA framework that is capable of handling both dense and sparse functional data.

Most previous works on the Bayesian FPCA model employed multivariate normal distribution to model the discretized, noise-contaminated observations. Despite the fact that the multivariate normal distribution has several desirable properties for modelling data, it is common that observations are not normally distributed in general. Various alternative distributions are available to accommodate higher moments. For instance, the multivariate Student- t distribution works well for fat-tailed data but does not consider asymmetry. The log-normal distribution has been used to model skewed data, but its skewness is reflected as a function of the mean and variance. This is somewhat inflexible because skewness is not a separate parameter. Branco and Dey (2001) proposed a general class of skew elliptical distributions by extending the previous work on a multivariate skew normal distribution as described by Azzalini and Valle (1996). The general class developed by Branco and Dey (2001) includes the multivariate normal, Student- t , and exponential power, but with an additional parameter to control skewness. This family of distributions was improved upon by Sahu et al. (2003) for capturing multivariate asymmetry and adding more flexibility in adjusting the correlation structure, which often leads to better-fitting models. Moreover, the family of distributions proposed by Sahu et al. (2003) offers a convenient implementation within a Bayesian framework.

Given the various advantages offered by Bayesian inference and the advancement of the skew elliptical class of distributions, we propose a general method to fit the observations with some multivariate skew elliptical distributions within the Bayesian FPCA framework. Our proposed method has three main advantages. First, our method produces more robust estimations of the covariance function and the corresponding principal components by integrating the class of skew elliptical distributions. In practice, many problems involve a proper transformation for symmetry for skewed data. Such ad hoc transformations can be avoided by using the proposed models. Rather than transforming the data, our methods transform error distributions to handle skewness. Second, adopting a Bayesian approach for

the FPCA problem facilitates the interpretation of uncertainty measures, such as credible intervals. This aligns with the inherent view of making a probability statement concerning the data after people have observed it. Finally, we extend our method to fit functional data that are sparsely and irregularly observed, making the Bayesian FPCA fully adapted to any type of functional data.

The rest of the article is organized as follows: We introduce the setup of Bayesian FPCA in Section 2.1. The proposed model is presented in Section 2.2, along with computational details in Section 2.3, a description of outlier detection method in Section 2.4, and an extension to sparse data in Section 2.5. Simulation studies are presented in Section 3, in which we compare the proposed model to other Bayesian and frequentist FPCA approaches in the presence of different data generation processes and noise levels. Three examples including dense and sparse data are discussed in Section 4. A summary and some directions for future work are given in Section 5.

2 Robust Bayesian FPCA

In this section, we will present the proposed robust Bayesian FPCA model and describe the features that contribute to its improvement over the existing FPCA methods.

2.1 Bayesian Functional Principal Component Analysis

Functional principal component analysis (FPCA) extends the idea of the principal component analysis of multivariate data (see Jolliffe, 2002, for a comprehensive introduction to classical multivariate PCA) to functional data. FPCA is the most prevalent tool in FDA and serves as a standard first step when processing functional data in most cases (Ramsay and Silverman, 2005a). This is due to FPCA's capability to convert inherently infinite-dimensional functional data into a finite-dimensional vector of random scores. The general goals of FPCA include finding patterns in data of high dimensions, capturing the major sources of variation and reducing the dimensionality.

Denote $\{X(t) : t \in [0, T] \in \mathcal{R}\}$ as a square integrable stochastic process. Consider

n independent and identically distributed realizations, $X_1(t), X_2(t), \dots, X_n(t)$, of a mean-zero stochastic process with covariance function $\text{Cov}_X(s, t)$ at a sequence of random points on $\mathcal{T} = [0, T]$. The covariance function $\text{Cov}_X(s, t)$ specifies the covariance between curve values $X_i(s)$ and $X_i(t)$ at times s and t , respectively. We assume the observations are noise-corrupted. That is, the observed data $Y_i^*(t_{ij}), i = 1, \dots, n, j = 1, \dots, n_i$, is

$$Y_i^*(t_{ij}) = \mu(t) + X_i(t_{ij}) + \epsilon_{ij}, \quad (1)$$

where $Y_i^*(t_{ij})$ is the discretized, noise-contaminated, observed data for every curve $i = 1, \dots, n$, at the time point t_{ij} ; $\mu(t)$ is the mean function; $X_i(t_{ij})$ is the true underlying detrended curve from a Gaussian process with mean zero and covariance function, i.e., $X_i(t) \sim \text{GP}(\mathbf{0}, \text{Cov}_X(s, t))$ for $s, t \in \mathcal{T}$, independently for $i = 1, \dots, n$; and ϵ_{ij} 's are the noise terms with $\mathbb{E}(\epsilon_{ij}) = 0$ and $\text{Var}(\epsilon_{ij}) = \sigma_{ij}^2$. We assume ϵ_{ij} are independent across i and j .

We first consider the case when the observed data $Y_i^*(t_{ij})$ are dense and equally spaced, i.e., the number of measurements n_i for each curve is the same and the sequence t_{i1}, \dots, t_{in_i} is equally spaced for every curve $i = 1, \dots, n$. Let $Y_i(t) = Y_i^*(t) - \hat{\mu}(t)$ be the detrended observations, where $\hat{\mu}(t) = \frac{1}{n} \sum_{i=1}^n Y_i^*(t)$.

Mercer's theorem states that, under mild assumptions, the spectral decomposition of the covariance function can be approximated as

$$\text{Cov}_X^K(s, t) = \sum_{k=1}^K \lambda_k \phi_k(s) \phi_k(t), \text{ for } s, t \in \mathcal{T}, \quad (2)$$

where $\text{Cov}_X^K(s, t)$ converges uniformly to $\text{Cov}_X(s, t)$ as $K \rightarrow \infty$, $\{\lambda_1, \lambda_2, \dots\}$ are the non-negative eigenvalues in non-increasing order of the covariance operator, and $\{\phi_1, \phi_2, \dots\}$ are the corresponding orthogonal eigenfunctions. We can simplify the notation for covariance function by defining $Q(s, t) = \text{Cov}_X^K(s, t)$ throughout the rest of the article. By the Karhunen-Loève expansion (Fukunaga and Koontz, 1970), each de-measured curve $X_i(t)$ can be approximated by a linear combination of the eigenfunctions $\phi_k(t)$ and FPC scores ξ_{ik} :

$$X_i(t) \approx \sum_{k=1}^K \xi_{ik} \phi_k(t). \quad (3)$$

By truncating the infinity expansion at some level, $K \in \mathbb{N}$, the resulting finitely truncated series provides a good approximation to $X_i(t)$.

The eigenfunctions $\{\phi_1, \phi_2, \dots\}$ can be further represented with the following basis expansion:

$$\phi_k(t) = \sum_{p=1}^{\infty} c_{kp} h_p(t) \approx \sum_{p=1}^P c_{kp} h_p(t), \quad (4)$$

where $h_p(t)$'s are some given basis functions and c_{kp} 's are the corresponding basis coefficients. The expansion in equation (4) is truncated at some level, $P \in \mathbb{N}$. Assigning priors on the truncating parameters P and K ensure full support. Let \mathbf{H}_P be the $T \times P$ matrix with columns consisting of the given basis functions evaluated at all points. Let \mathbf{C}_{KP} denote the coefficient matrix of size $K \times P$ and $\mathbf{\Lambda}_K$ be a $K \times K$ diagonal matrix whose diagonal is composed of the non-negative eigenvalues $\{\lambda_1, \lambda_2, \dots, \lambda_K\}$ in non-increasing order. Then the covariance function can be represented by the following relation:

$$Q(s, t) = \mathbf{H}'_P(s) \mathbf{C}'_{KP} \mathbf{\Lambda}_K \mathbf{C}_{KP} \mathbf{H}_P(t), \text{ for } s, t \in \mathcal{T}. \quad (5)$$

2.2 Models and Prior Specification

In this section, we give details on the structure of the proposed robust Bayesian FPCA (RB-FPCA) method and features that improve the previous Bayesian FPCA model in Suarez and Ghosal (2017). The prior on the covariance function $Q(s, t)$ in Equation 5 will be specified indirectly on $\mathbf{\Omega}^{-1} = (\mathbf{C}'_{KP} \mathbf{\Lambda}_K \mathbf{C}_{KP})^{-1}$, and the prior is assumed to be a Wishart distribution. When the number of principal components (K) is less than the number of basis functions (P) used for approximation, the Wishart matrix becomes singular (Uhlig, 1994). Because the Wishart distribution gives zero density to singular matrices, to allow the constraint of $K \leq P$, it is necessary to consider the inclusion of singular Wishart matrices into the specification of the prior.

Let $\mathbf{\Psi} = \mathbf{U} \mathbf{L} \mathbf{U}'$, where \mathbf{U} is a $P \times P$ orthogonal matrix and \mathbf{L} is a $P \times P$ diagonal matrix with ordered eigenvalues along the diagonal. Now define $\mathbf{\Psi}_K = \mathbf{U}_K \mathbf{L}_K \mathbf{U}'_K$, where \mathbf{U}_K is the first K columns of \mathbf{U} and \mathbf{L}_K is the first K rows and K columns of \mathbf{L} . It follows that $\mathbf{\Psi}_K$ has rank K even though its dimension is $P \times P$. By defining the singular center matrix

Ψ_K of rank K , we allow for singular Wishart matrices in specifying the prior (see Suarez and Ghosal (2017)). For any random matrix \mathbf{S} , a Moore-Penrose inverse of \mathbf{S} is defined as a matrix \mathbf{S}^+ . Suppose that $\mathbf{S}_1 \sim \text{Wishart}_P(\nu, \Psi_K^+)$ and $\mathbf{S}_2 \sim \text{Wishart}_K(\nu, \mathbf{L}_k^{-1})$, then

$$\begin{aligned}\mathbf{S}_1 &\stackrel{D}{\rightarrow} \mathbf{U}_K \mathbf{S}_2 \mathbf{U}'_K, \\ \mathbf{S}_1^+ &\stackrel{D}{\rightarrow} \mathbf{U}_K \mathbf{S}_2^{-1} \mathbf{U}'_K.\end{aligned}$$

This property forms the desired singularity in the prior specification.

The model proposed in this work differs from that of Suarez and Ghosal (2017) who model the discretized observations with multivariate normal distribution. We propose to fit multivariate skew elliptical distributions to model the observations, which produces more robust estimates in the Bayesian FPCA framework. To construct the skew elliptical class of distributions, we first present the general settings for multivariate symmetric elliptical distributions, followed by an introduction to the general skew elliptical class of distributions, where skewness is induced via transformation and conditioning.

Let $\boldsymbol{\epsilon}$ and \mathbf{z} be two T -dimensional random vectors. Let $\boldsymbol{\mu}$ denote an T -dimensional vector and $\boldsymbol{\Sigma}$ denote an $T \times T$ positive definite matrix. We will use the following notation to represent the general class of elliptically symmetric distributions:

$$\boldsymbol{\eta} = \begin{pmatrix} \boldsymbol{\epsilon} \\ \mathbf{z} \end{pmatrix} \sim \text{El} \left(\begin{pmatrix} \boldsymbol{\mu} \\ \mathbf{0} \end{pmatrix}, \begin{bmatrix} \boldsymbol{\Sigma} & \mathbf{0} \\ \mathbf{0} & \mathbf{I} \end{bmatrix}; g^{(2T)} \right), \quad (6)$$

where $\mathbf{0}$ and \mathbf{I} are the null matrix and identity matrix, respectively, and $g^{(2T)}$ is the generator of the probability density function (PDF). Note that the generator $g^{(2T)}$ depends on the dimensions of the random vector $\boldsymbol{\eta} = (\boldsymbol{\epsilon}', \mathbf{z}')'$, and $2T$ is the dimension of $\boldsymbol{\eta}$. The density generator $g^{(2T)}$ is a function from \mathbb{R}^+ to \mathbb{R}^+ which satisfies

$$\int_0^\infty w^{T-1} g^{(2T)}(w) dw = \pi^{-T} \Gamma(T), \quad (7)$$

where $\Gamma(T) = (T-1)!$ is the gamma function. The choice of the density generator function will determine the distribution of the random vector. This flexible nature of the elliptical class of distributions allows for including several widely recognized symmetric distributions as proper members, for example, the multivariate normal distribution. Assume a random

vector $\boldsymbol{\eta}$ of dimension $2T$ follows a multivariate Normal distribution with mean vector $\boldsymbol{\mu}$ and covariance matrix $\boldsymbol{\Sigma}$, i.e., $\boldsymbol{\eta} \sim MVN(\boldsymbol{\mu}, \boldsymbol{\Sigma})$, the probability density function can be formulated via the following generalized expression in terms of the generator function $g^{(2T)}$:

$$f(\boldsymbol{\eta} \mid \boldsymbol{\mu}, \boldsymbol{\Sigma}; g^{(2T)}) = |\boldsymbol{\Sigma}|^{-1/2} g^{(2T)}((\boldsymbol{\eta} - \boldsymbol{\mu})' \boldsymbol{\Sigma}^{-1} (\boldsymbol{\eta} - \boldsymbol{\mu})),$$

where the density generator function has the form of $g^{(2T)}(u) = e^{-u/2}/(2\pi)^T$. The conventional form of the multivariate normal distribution's PDF can be retrieved with this density generator function.

Next, we consider a general skew elliptical class of distributions by implementing the transformation presented in Sahu et al. (2003):

$$\mathbf{Y} = \mathbf{D}\mathbf{z} + \boldsymbol{\epsilon}, \tag{8}$$

where \mathbf{Y} is the transformed variable which followed the skew elliptical distribution, and \mathbf{D} is a diagonal matrix with diagonals $\mathbf{d} = (d_1, \dots, d_T)'$, which accommodates skewness. Let $\text{vec}(\mathbf{D})$ denote a vector of diagonals of \mathbf{D} . The skew elliptical class is developed by considering the random variable $\mathbf{Y} \mid \mathbf{z} > 0$, where $\mathbf{z} = (z_1, \dots, z_T)'$ > 0 implies every element of \mathbf{z} is positive. The construction in equation (8) along with the conditioning introduces skewness. Specifically, positive values of elements of \mathbf{d} result in positively skewed distributions, while negative values lead to negatively skewed distributions. Note that the elliptically symmetric distribution is retrieved if the diagonals of \mathbf{D} are zeros, i.e., $d_1, \dots, d_T = 0$. With the transformation and conditioning, the random variable \mathbf{Y} follows the skew elliptical distribution and we denote it with the notation $\mathbf{Y} \sim SE(\boldsymbol{\mu}, \boldsymbol{\Sigma}, \mathbf{D}; g^{(T)})$. We will consider one example of the skew elliptical class of distributions throughout this paper, namely the multivariate skew normal distribution.

We can now integrate the family of skew elliptical distributions within the Bayesian FPCA framework and present the full RB-FPCA model. Let $\mathbf{Y}_i = (Y_i(t))'$ for $i = 1, \dots, n$. We assume $\mathbf{Y}_i \sim SE(\boldsymbol{\mu}_i, \boldsymbol{\Sigma}, \mathbf{D}; g^{(n_i)})$, and further relax the assumption of homoscedasticity on noises. The hierarchical representation of the proposed RB-FPCA model for $i = 1, \dots, n$,

is

$$\begin{aligned}
\mathbf{Y}_i | \cdot &\sim MVN_T(\mathbf{H}_P \mathbf{U}_K \boldsymbol{\beta}_{i,K} + \mathbf{D} \mathbf{z}_i, \boldsymbol{\Sigma}), \\
\boldsymbol{\beta}_{i,K} &\stackrel{i.i.d}{\sim} MVN_K(\mathbf{0}, \boldsymbol{\Omega}), \\
\boldsymbol{\Omega}^{-1} &\sim Wishart_K(\nu, \mathbf{L}_k^{-1}), \\
\mathbf{z}_i &\sim MVN_T(\mathbf{0}, \mathbf{I}) I(\mathbf{z}_i > 0), \\
\text{vec}(\mathbf{D}) &\sim MVN_T(\mathbf{0}, \boldsymbol{\Gamma}), \\
\boldsymbol{\Sigma}^{-1} &\sim Wishart_T(2r, 2\boldsymbol{\kappa}),
\end{aligned}$$

where $\nu, \boldsymbol{\Gamma}, 2r$ and $\boldsymbol{\kappa}$ are hyperparameters. This proposed model takes singular Wishart matrices into account in the prior specification because $\mathbf{U}_K \boldsymbol{\Omega}^{-1} \mathbf{U}'_K \sim Wishart_P(\nu, \boldsymbol{\Psi}_K^+)$. The main purpose of the inference is to estimate the covariance function and the principal components from the data. More specifically, the covariance function of interest is $\mathbf{H}'_P(s) \mathbf{U}'_K \boldsymbol{\Omega} \mathbf{U}_K \mathbf{H}_P(t)$ and the principal components it induces are $\mathbf{C}_{KP} \mathbf{H}'_P(t)$.

2.3 Posterior Inference

Our goal is to sample the parameters from the posterior distribution by deriving their full conditional distributions. All parameters' conditional distributions can be derived analytically in closed forms and are given as follows. In each conditional distribution, we use $|\dots$ to denote conditioning on the data and all other parameters.

- For $i = 1, \dots, n$, the full conditional distribution for $\boldsymbol{\beta}_{i,K}$ is

$$\begin{aligned}
\boldsymbol{\beta}_{i,K} | \dots &\sim MVN_K((\mathbf{U}'_K \mathbf{H}'_P \boldsymbol{\Sigma}^{-1} \mathbf{H}_P \mathbf{U}_K + \boldsymbol{\Omega}^{-1})^{-1} (\mathbf{U}'_K \mathbf{H}'_P \boldsymbol{\Sigma}^{-1} \mathbf{Y}_i), \\
&(\mathbf{U}'_K \mathbf{H}'_P \boldsymbol{\Sigma}^{-1} \mathbf{H}_P \mathbf{U}_K + \boldsymbol{\Omega}^{-1})^{-1}),
\end{aligned} \tag{9}$$

where \mathbf{H}_P is picked to be the Legendre polynomial basis functions and the choice of \mathbf{U}_K is discussed in the conditional distribution for $\boldsymbol{\Omega}^{-1}$.

- For $\boldsymbol{\Omega}^{-1}$, the full conditional distribution is

$$\boldsymbol{\Omega}^{-1} | \dots \sim Wishart_K(\nu + n + 1, (\mathbf{L}_k + \sum_{i=1}^n \boldsymbol{\beta}_{i,K} \boldsymbol{\beta}'_{i,K})^{-1}), \tag{10}$$

where ν is the number of degrees of freedom. A sensible choice of Ψ is given as $\Psi = (\mathbf{H}'_P \mathbf{H}_P)^{-1} \mathbf{H}'_P \mathbf{\Omega}^* \mathbf{H}_P (\mathbf{H}'_P \mathbf{H}_P)^{-1}$, where $\mathbf{\Omega}^*$ is the prior covariance function corresponding to the time grid being used. \mathbf{U}_K and \mathbf{L}_K are obtained by decomposing Ψ and subsetting the resulting matrices \mathbf{U} and \mathbf{L} as described in Section 2.2.

- For \mathbf{z}_i , the full conditional distribution is

$$\mathbf{z}_i | \dots \sim MVN_T(\mathbf{A}_i^{-1} \mathbf{a}_i, \mathbf{A}_i^{-1}) I(\mathbf{z}_i > 0), \quad (11)$$

where $\mathbf{A}_i = \mathbf{I} + \mathbf{D} \mathbf{\Sigma}^{-1} \mathbf{D}$ and $\mathbf{a}_i = \mathbf{D} \mathbf{\Sigma}^{-1} (\mathbf{Y}_i - \mathbf{H}_P \mathbf{U}_K \boldsymbol{\beta}_{i,K})$.

- For $\text{vec}(\mathbf{D})$, the full conditional distribution is

$$\text{vec}(\mathbf{D}) | \dots \sim MVN_T(\mathbf{B}^{-1} \mathbf{b}, \mathbf{B}^{-1}), \quad (12)$$

with $\mathbf{B} = \mathbf{\Gamma}^{-1} + \sum_{i=1}^n \text{diag}(\mathbf{z}_i) \mathbf{\Sigma}^{-1} \text{diag}(\mathbf{z}_i)$, $\mathbf{b} = \sum_{i=1}^n \text{diag}(\mathbf{z}_i) \mathbf{\Sigma}^{-1} (\mathbf{Y}_i - \mathbf{H}_P \mathbf{U}_K \boldsymbol{\beta}_{i,K})$.

- For $\mathbf{\Sigma}^{-1}$, the full conditional distribution is

$$\begin{aligned} \mathbf{\Sigma}^{-1} | \dots \sim & \text{Wishart}_T(2r + n, ((2\boldsymbol{\kappa})^{-1} + \\ & \sum_{i=1}^n (\mathbf{Y}_i - \mathbf{H}_P \mathbf{U}_K \boldsymbol{\beta}_{i,K} - \mathbf{D} \mathbf{z}_i) (\mathbf{Y}_i - \mathbf{H}_P \mathbf{U}_K \boldsymbol{\beta}_{i,K} - \mathbf{D} \mathbf{z}_i)')^{-1}). \end{aligned} \quad (13)$$

The conditional distributions for all parameters of interest are readily accessible in closed forms, we therefore employ a Gibbs sampling algorithm to sample from the posterior distribution. The algorithm samples new values for each parameter iteratively based on the current values of the other unknown parameters. Some advantages of the Gibbs sampling algorithm include its simplicity and fast convergence in our implementation. For posterior inference, the covariance function is estimated with the full posterior mean. The principal components $\hat{\phi}_k(t)$ are estimated by decomposing the estimated posterior mean of the covariance function. The corresponding FPC scores are estimated with $\hat{\xi}_{ik} = \int_{\mathcal{T}} \hat{\phi}_k(t) Y_i(t) dt$.

Next, we will discuss possible approaches to determine the number of eigenfunctions K , which gives a reasonably good approximation to the infinite-dimensional functional data. Model comparison through Bayes factors (Jeffreys, 1935; Han and Carlin, 2001) is a standard way for selecting models in the Bayesian framework. The calculation of the

Bayes factor requires estimating the marginal likelihood, which is the normalization factor of the posterior density. There has been great difficulty in obtaining the marginal likelihood estimates, which poses a challenge to the computation of the Bayes factor. We employed the method by Chib (1995), and the marginal likelihood estimates can be easily obtained since all conditional distributions in the Gibbs sampling algorithm have closed-form expressions. For more efficient computing, another straightforward approach is to select the number of eigenfunctions K which can explain a sufficiently large part of the total variation. We predetermined the value of K in all simulation studies and data analysis, and results showed that the first four eigenfunctions are able to explain at least 95% of the total variability in the data in all cases.

2.4 Outlier Detection

The estimated FPC scores can be used to detect any potential outlying trajectories. We employ a robust outlier detection approach described in Boente and Salibián-Barrera (2021). The first step is calculating the robust estimates for multivariate location and scatter of the estimated FPC scores. These estimates, named MM-estimates proposed by Yohai (1987), have a high breakdown point while remaining efficient. The breakdown point is a measure of robustness, defined as the maximum proportion of contamination or atypical points the data may contain while the estimator remains informative about the underlying parameter. Thus, estimators with higher breakdown-point are desired. Then we compute the robust Mahalanobis distance, which is defined as

$$d_{\text{Mahalanobis}}(\hat{\boldsymbol{\xi}}_i) = \sqrt{(\hat{\boldsymbol{\xi}}_i - \hat{\boldsymbol{\mu}}_{MM})' \hat{\boldsymbol{\Sigma}}_{MM}^{-1} (\hat{\boldsymbol{\xi}}_i - \hat{\boldsymbol{\mu}}_{MM})},$$

where $\hat{\boldsymbol{\xi}}_i = (\hat{\xi}_{i1}, \dots, \hat{\xi}_{iK})'$, $\hat{\boldsymbol{\mu}}_{MM}$ and $\hat{\boldsymbol{\Sigma}}_{MM}$ denote the MM-estimators for multivariate location and scatter, respectively. The trajectory i is flagged as an outlier if its FPC scores have a distance larger than a threshold quantile of a χ_K^2 distribution. Different threshold values can be applied to detect mild and extreme outliers.

2.5 Extend to Sparse Longitudinal Data

In this section, we extend the robust Bayesian FPCA model in 2.2 to fit longitudinal data that are sparsely and irregularly observed. We assume the observations are contaminated by measurement errors and adopt the FDA model given in equation 1. Now we consider the case when the number of measurements n_i made per subject is random due to the sparse and irregular designs. We also assume that the random variables n_i are i.i.d. The sparse data are centered before fitting the RB-FPCA model, i.e., $Y_i(t_{ij}) = Y_i^*(t_{ij}) - \hat{\mu}(t)$ for $i = 1, \dots, n$, $j = 1, \dots, n_i$. The mean function $\mu(t)$ can be estimated based on the pooled data from all individuals.

Write $\mathbf{Y}_i = (Y_i(t_{i1}), \dots, Y_i(t_{in_i}))'$. The hierarchical representation of the proposed RB-FPCA model for $i = 1, \dots, n$ with sparse longitudinal data is

$$\begin{aligned} \mathbf{Y}_i \mid \cdot &\sim MVN_{n_i}(\mathbf{H}_P^{(i)} \mathbf{U}_K^{(i)} \boldsymbol{\beta}_{i,K} + \mathbf{D}^{(i)} \mathbf{z}^{(i)}, \boldsymbol{\Sigma}^{(i)}), \\ \boldsymbol{\beta}_{i,K} &\stackrel{i.i.d.}{\sim} MVN_K(\mathbf{0}, \boldsymbol{\Omega}), \\ \boldsymbol{\Omega}^{-1} &\sim Wishart_K(\nu, \mathbf{L}_k^{-1}), \\ \mathbf{z}^{(i)} &\sim MVN_{n_i}(\mathbf{0}, \mathbf{I}) I(\mathbf{z}^{(i)} > 0), \\ \text{vec}(\mathbf{D}^{(i)}) &\sim MVN_{n_i}(\mathbf{0}, \boldsymbol{\Gamma}^{(i)}), \\ (\boldsymbol{\Sigma}^{(i)})^{-1} &\sim Wishart_{n_i}(2r, 2\boldsymbol{\kappa}^{(i)}), \end{aligned}$$

where the superscript (i) represents the parameters whose values and dimensions depend on the curve index i . The full conditional distributions in the Gibbs sampling for the sparse longitudinal data have similar forms except for the hyperparameter $\mathbf{R}^{(i)}$ in the conditional distribution of $\boldsymbol{\Sigma}^{-1}$, which is defined as a $n_i \times n_i$ diagonal matrix where elements of the main diagonal are the squared ranges of the corresponding components in the data. For the sparse longitudinal data, the squared ranges of the components cannot be directly calculated since data are observed at different time points. We estimate the squared ranges with a search bandwidth denoted as h_R , and a default value $h_R = 0.05n$ is used in all simulations and examples. Specifically, a set of h_R observations that are closest to the target observation will be used to estimate the squared ranges for the target individual at a specific time point. Furthermore, to ensure the matrix $\boldsymbol{\Psi}$ described in the full conditional

distribution of $\boldsymbol{\Omega}^{-1}$ is valid, we assume the number of principal components is less than or equal to the number of basis functions, and the number of basis functions used for approximation is less than or equal to the minimum number of observations per subject, i.e., $K \leq P \leq \min(1, \dots, n_i)$.

The posterior covariance function is $\mathbf{H}'_P(s)\mathbf{U}'_K\boldsymbol{\Omega}\mathbf{U}_K\mathbf{H}_P(t)$, where \mathbf{H}_P and \mathbf{U}_K are constructed using a given number of support points in each direction of the covariance surface. The default value of support points is set as 51 (same as in `fdapace` package in R). The principal components are $\mathbf{C}_{KP}\mathbf{H}'_P(t)$. The traditional way to estimate the FPC scores with numerical integration is used and performs well when a sufficiently dense measurement grid for each subject is available. However, when dealing with sparse longitudinal data, the numerical integration approximated by sums could not produce reasonable approximations due to the sparseness of the data. Thus, the alternative PACE method described by Yao et al. (2005) is implemented here to find FPC scores for sparse longitudinal data. Specifically, using the data from each subject, the prediction of the FPC scores for the i th subject is given by the conditional expectation:

$$\hat{\xi}_{ik} = \hat{\mathbb{E}}[\xi_{ik}|\mathbf{Y}_i] = \hat{\lambda}_k\hat{\phi}'_{ik}(t)\hat{Q}_{\mathbf{Y}_i}^{-1}\mathbf{Y}_i, \quad (14)$$

where $\hat{\lambda}_k$ is the k th estimated eigenvalues of $\hat{Q}(s, t)$, $\hat{\phi}_{ik}(t)$ is the estimates of the eigenfunctions $\phi_{ik}(t) = (\phi_k(t_{i1}), \dots, \phi_k(t_{in_i}))'$, and the (j, l) th element of $\hat{Q}_{\mathbf{Y}_i}$ is $(\hat{Q}_{\mathbf{Y}_i})_{j,l} = \hat{Q}(t_{ij}, t_{il}) + \hat{\boldsymbol{\Sigma}}^{(i)}$. This conditioning method works with sparse data with the existence of measurement errors and gives the best prediction of the FPC scores under Gaussian assumptions. The estimate $\hat{\xi}_{ik}$ in equation 14 is the best linear prediction of ξ_{ik} from the information in the i th subject, regardless of whether the Gaussian assumption holds (as previously observed in Yao et al. (2005)).

3 Simulation Studies

3.1 Simulation I: Dense functional data without outliers

In the first simulation, we aim to compare the performance of the proposed RB-FPCA method with different frequentist and Bayesian FPCA methods. We followed a similar

simulation setting as in Suarez and Ghosal (2017). Each set of simulated data consists of 20 noisy observations over 50 time points. These time points are evenly spaced in the interval $[-1, 1]$. The underlying true mean function is $\mu(t) = \sin(2\pi t)$. Depending on the experimental settings, the true underlying covariance function is of either $\text{Cov}_1(s, t) = \exp\{-3(t - s)^2\}$ or $\text{Cov}_2(s, t) = \min\{s + 1, t + 1\}$. Next, independent noise is added to the sampling process in the form of $N(0, 0.3)$ random variables.

The four methods for comparison are listed below:

- i. our proposed robust Bayesian FPCA (RB-FPCA) method
- ii. Bayesian FPCA (BFPCA) method of Suarez and Ghosal (2017)
- iii. Fast Covariance Estimation (FACE) method of Xiao et al. (2016), implemented in `refund` package in R
- iv. Principal Analysis by Conditional Estimation (PACE) method of Wang et al. (2016), implemented in `fdapace` package in R

In RB-FPCA and BFPCA methods, we predetermined the numbers of basis functions and eigenfunctions as $P = 15$ and $K = 5$. We established the values for the hyperparameters as outlined in Sahu et al. (2003). We set $\nu = 2K$ for $\mathbf{\Omega}^{-1}$ in equation 10, $\mathbf{\Gamma} = \text{diag}(10, \dots, 10)$ for $\text{vec}(\mathbf{D})$ in equation 12, $2r = T$ and $\boldsymbol{\kappa} = 100 * \mathbf{R}^{-1}/(2r)$ for $\mathbf{\Sigma}^{-1}$ in equation 13. \mathbf{R} is a diagonal matrix of dimensions $T \times T$, wherein the main diagonal elements are the squared ranges of the corresponding components in the data. These chosen hyperparameter values yield satisfactory results in the simulation studies and are consistently employed in all examples unless explicitly stated otherwise. We compared the methods in the following aspects with different metrics: estimation of the covariance function with L_2 norms and estimation of the principal components with mean squared errors. Each simulation represents a choice between $\text{Cov}_1(s, t)$ and $\text{Cov}_2(s, t)$ as the true covariance function and the prior covariance function, which results in four experimental settings. For each setting, a total of 10000 iterations is run and we discard the first 5000 as the burn-in and use the remainder 5000 for inference. Each setting is repeated 30 times

with different seeds and the results are the average of the estimated posterior means from 30 runs.

	Truth	Prior	RB-FPCA	BFPCA	FACE	PACE	pct(RB-FPCA is best)
Covariance	Cov1	Cov1	11.857	13.981	13.609	17.288	0.67
		Cov2	12.864	15.239			
Function	Cov2	Cov1	14.163	17.135	14.545	17.209	0.53
		Cov2	13.288	16.435			

Table 1: Simulation I: Estimations of the covariance function are evaluated by the L_2 norm.

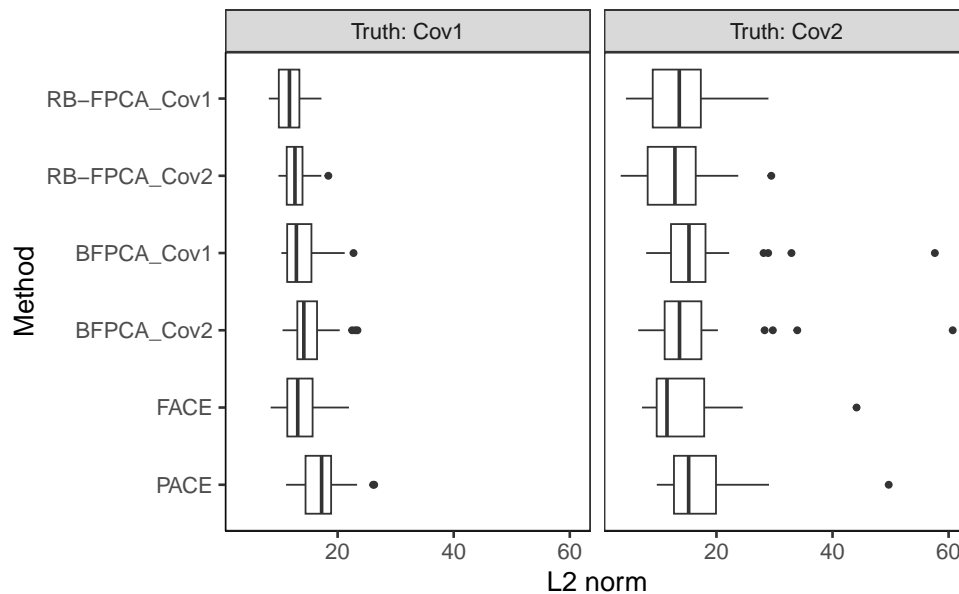


Figure 2: Simulation I: Boxplots of L_2 norms between the estimates and the true covariance function.

From Table 1 and Figure 2, covariance functions are estimated well by the proposed RB-FPCA method under the condition that the true covariance function is $\text{Cov}_1(s, t)$. The proposed RB-FPCA method has a competitive performance against the two frequentist methods, given that the true covariance function is $\text{Cov}_2(s, t)$. Generally, a prior covariance function constructed based on the true covariance function can enhance estimation. Some

	Truth	Prior	RB-FPCA	BFPCA	FACE	PACE	pct(RB-FPCA is the best)
PC1	Cov1	Cov1	0.041	0.044	0.043	0.039	0.50
		Cov2	0.048	0.046			
	Cov2	Cov1	0.017	0.019	0.037	0.046	0.30
		Cov2	0.035	0.035			
PC2	Cov1	Cov1	0.028	0.029	0.045	0.048	0.63
		Cov2	0.040	0.041			
	Cov2	Cov1	0.036	0.046	0.033	0.041	0.20
		Cov2	0.029	0.028			
PC3	Cov1	Cov1	0.026	0.027	0.031	0.040	0.50
		Cov2	0.051	0.055			
	Cov2	Cov1	0.024	0.021	0.032	0.038	0.40
		Cov2	0.042	0.047			

Table 2: Simulation I: Estimations of the first 3 principal components are compared with Mean Squared Errors (MSEs).

certain degrees of subject matter expertise in the structure of the covariance function can be incorporated into the analysis to improve the estimation further. The estimations of the principal components measured by MSEs in Table 2 also indicate that the proposed RB-FPCA method can provide comparable performance to the BFPCA and some well-known frequentist methods.

3.2 Simulation II: Dense functional data with outliers

The second simulation considers the presence of outliers. The goal is to investigate the finite-sample performance and robustness of the proposed model. Different percentages of atypical observations are considered. A total of 100 observations over 50 time points are generated in each case.

For clean observations, the data are generated from the following model:

$$Y_i(t) = \mu(t) + \sum_{k=1}^K \sqrt{\lambda_k} Z_{i,k} \phi_k(t), \quad i = 1, \dots, n, \quad (15)$$

with $Z_{i,k} \stackrel{i.i.d}{\sim} \mathcal{N}(0, 1)$ and eigenvalues $\lambda_1 \geq \lambda_2 \geq \dots \geq \lambda_K > 0$. Time points are evenly spaced in the interval $[0, 1]$. The mean function is set to $\mu(t) = 10 \sin(2\pi t) \exp(-3t)$. We set $K = 4$ and choose the eigenfunctions $\phi_k(t)$ as the first K eigenfunctions of the Matérn Covariance function (Rasmussen, 2003):

$$\text{COV}_{\text{Matérn}}(s, t) = \sigma^2 \frac{2^{1-\nu}}{\Gamma(\nu)} \left(\frac{\sqrt{2\nu}|s-t|}{\rho} \right)^\nu K_\nu \left(\frac{\sqrt{2\nu}|s-t|}{\rho} \right),$$

where $\Gamma(\cdot)$ is the Gamma function and K_ν is a modified Bessel function of the second kind. We set the parameters as $\sigma^2 = 1$, $\rho = 3$, and $\nu = 1/2$. The eigenvalues $\lambda_1 = 0.83$, $\lambda_2 = 0.08$, $\lambda_3 = 0.03$, and $\lambda_4 = 0.015$ were selected so that they have similar ratios to those of the first four eigenvalues of the Matérn covariance function. In this model, the first principal direction summarizes major sources of variation among the curves. At the same time, the third and fourth eigenfunctions will tend to add some complexity to the covariance function.

To add outliers to the clean observations, we introduced atypical observations to change the order of the principal directions to affect the estimated eigenvalues and eigenfunctions. We added outliers with a Bernoulli random variable $B_i \sim \text{Bernoulli}(1, p)$, where p corresponds to the percentage of outliers. We contaminated the clean observations as follows:

- i. For curve i , generate the Bernoulli random variable B_i . If $B_i = 0$, then proceed to
 - (a). If $B_i = 1$, then proceed to (b).
 - (a) Generate the curve $Y_i(t)$ as described in equation 15
 - (b) Introduce outliers by altering the order of the principal directions. Sample the scores for the second and third principal directions with

$$\begin{pmatrix} Z_{i,2} \\ Z_{i,3} \end{pmatrix} \sim MVN_2 \left(\begin{pmatrix} 20 \\ 25 \end{pmatrix}, \begin{bmatrix} 1/16 & 0 \\ 0 & 1/16 \end{bmatrix} \right).$$

- ii. Repeat step i for all curves, $i = 1, \dots, n$.

Figure 3 shows one example of the 100 observations generated over 50 time points with an outlier percentage of $p = 0.1$. This figure illustrates how contamination alters the pattern

of the clean data. Black lines represent the clean samples, and blue lines correspond to 10 outlying samples.

We examined the behaviour of the estimated covariance function and the eigenfunctions for both clean and contaminated samples with $p = 0.05, 0.10, 0.15$. Each value of p is repeated 30 times with different seeds, and the final results are the average of the estimated posterior means from 30 runs. The prior covariance function used in this simulation is $\text{Cov}(s, t) = \exp\{-3(t - s)^2\}$. The numbers of basis functions and eigenfunctions are set to $P = 15$ and $K = 4$.

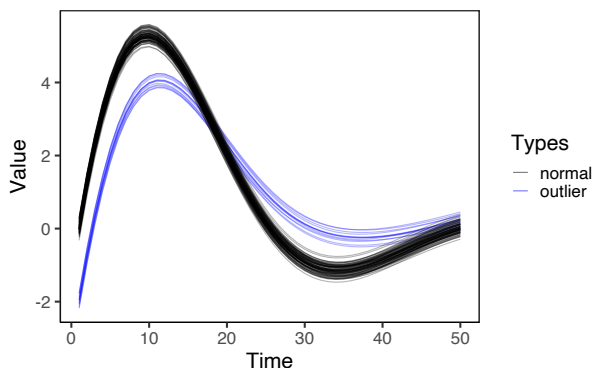
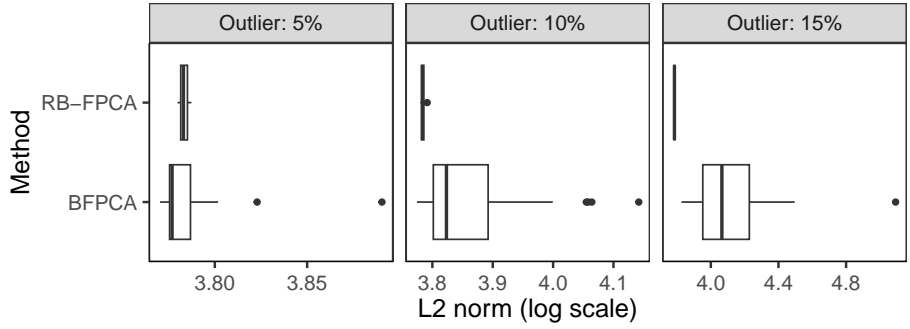


Figure 3: Simulation II: Clean samples with contaminated samples from the data generation process described in 3.2. The outlier percentage is 10%.

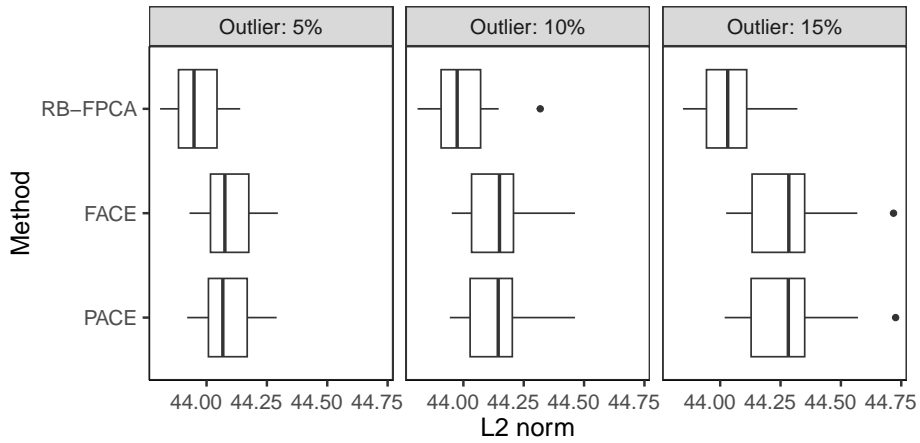
	p	RB-FPCA	BFPCA	FACE	PACE	pct(RB-FPCA is best)
Covariance Function	0.05	43.956	44.057	44.082	44.074	0.30
	0.10	43.991	48.131	44.141	44.135	0.93
	0.15	44.035	64.065	44.271	44.269	1.00

Table 3: Simulation II: Estimations of the covariance function are evaluated by the L_2 norms.

Table 3 compares the estimations of the covariance function in terms of the L_2 norms with varying outlier percentages, averaged across 30 replications. It can be observed that RB-FPCA shows significant improvement over BFPCA, providing a smaller error, and a moderate improvement over the two modern frequentist methods. Figures 4a and 4b display



(a)



(b)

Figure 4: Simulation II: (a) Boxplots of L_2 norms (in log scale) between the estimates and the true covariance function. Comparison is between the proposed RB-FPCA method and the other Bayesian methods. (b) Boxplots of L_2 norms between the estimates and the true covariance function. Comparison is between the proposed RB-FPCA method and the two frequentist methods.

	p	PCs	RB-FPCA	BFPCA	FACE	PACE
PCs	0.05	PC1	1.539	1.613	1.601	1.541
		PC2	1.463	1.464	1.590	1.554
		PC3	2.257	2.041	2.495	1.382
	0.10	PC1	1.572	1.574	1.593	1.549
		PC2	1.294	1.503	1.568	1.552
		PC3	2.083	2.234	2.489	1.507
	0.15	PC1	1.556	1.572	1.584	1.558
		PC2	1.244	1.497	1.569	1.565
		PC3	2.027	2.346	2.487	1.568

Table 4: Simulation II: Estimations of the first 3 principal components are compared with angles (in radians) between the truth and estimates.

the comparison of the boxplots of the L_2 norms. These boxplots confirm that RB-FPCA outperforms the other three methods in terms of median and dispersion. We also observe that the better performance of RB-FPCA is more pronounced when the outlier percentage is high. Table 4 summarizes the PC estimation results for various outlier percentage values. We can see that RB-FPCA outperforms BFPCA and FACE in estimating all the first 3 PCs and has a competitive performance compared with PACE.

3.3 Simulation III: Sparse functional data with outliers

The third simulation examines the performance of the Bayesian FPCA on the sparse longitudinal data. Each time we first generated a dense dataset with 100 noisy observations over 50 time points with the true mean function $\mu(t) = \sin(2\pi t)$. The true underlying covariance function is of either $\text{Cov}_1(s, t) = \exp\{-3(t - s)^2\}$ or $\text{Cov}_2(s, t) = \min\{s + 1, t + 1\}$ depending on the experimental settings. Outlier percentage is chosen from 5%, 10% or 15% with equal probability. For outliers, noises of $N(0, 3)$ are added to the sampling process. For clean samples, a small amount of noise of $N(0, 0.3)$ is added. To get sparsely observed samples, a discrete uniform distribution $U(5, 10)$ was used to select a random number of times n_i each curve was observed. The observed times t_{ij} satisfy $t_{ij} \sim U(-1, 1)$, i.i.d. for $i =$

$1, \dots, 100, j = 1, \dots, n_i$. This data generation process produces sparse longitudinal data with some noisy samples.

We tested the performance of our proposed RB-FPCA method with different prior covariance functions. When the true covariance function is $\text{Cov}_{truth}(s, t) = \exp\{-3(t-s)^2\}$, we set prior covariance functions with the following forms:

- $\text{Cov}_{prior1}(s, t) = \exp\{-3(t-s)^2\}$ (same as truth)
- $\text{Cov}_{prior2}(s, t) = \min(s+1, t+1)$
- $\text{Cov}_{prior3}(s, t) = \exp\{-(t-s)^2\}$
- $\text{Cov}_{prior4}(s, t) = \text{covariance estimation from PACE method}$

When the true covariance function is $\text{Cov}_{truth}(s, t) = \min(s+1, t+1)$, we set prior covariance functions with the following forms:

- $\text{Cov}_{prior1}(s, t) = \exp\{-3(t-s)^2\}$
- $\text{Cov}_{prior2}(s, t) = \min(s+1, t+1)$ (same as truth)
- $\text{Cov}_{prior3}(s, t) = (s+1) * (t+1)$
- $\text{Cov}_{prior4}(s, t) = \text{covariance estimation from PACE method}$

Figure 5 shows the contour plots of covariance functions. For each setting, we selected four prior covariance functions with different characteristics that may have an effect on the performance of the RB-FPCA method. Specifically, except for using the true covariance function as the prior covariance function, we also included one prior covariance function, which has a similar surface structure as the true covariance function and one prior covariance function with a different shape. In addition, we also involved the smoothed covariance surface estimated from the PACE method.

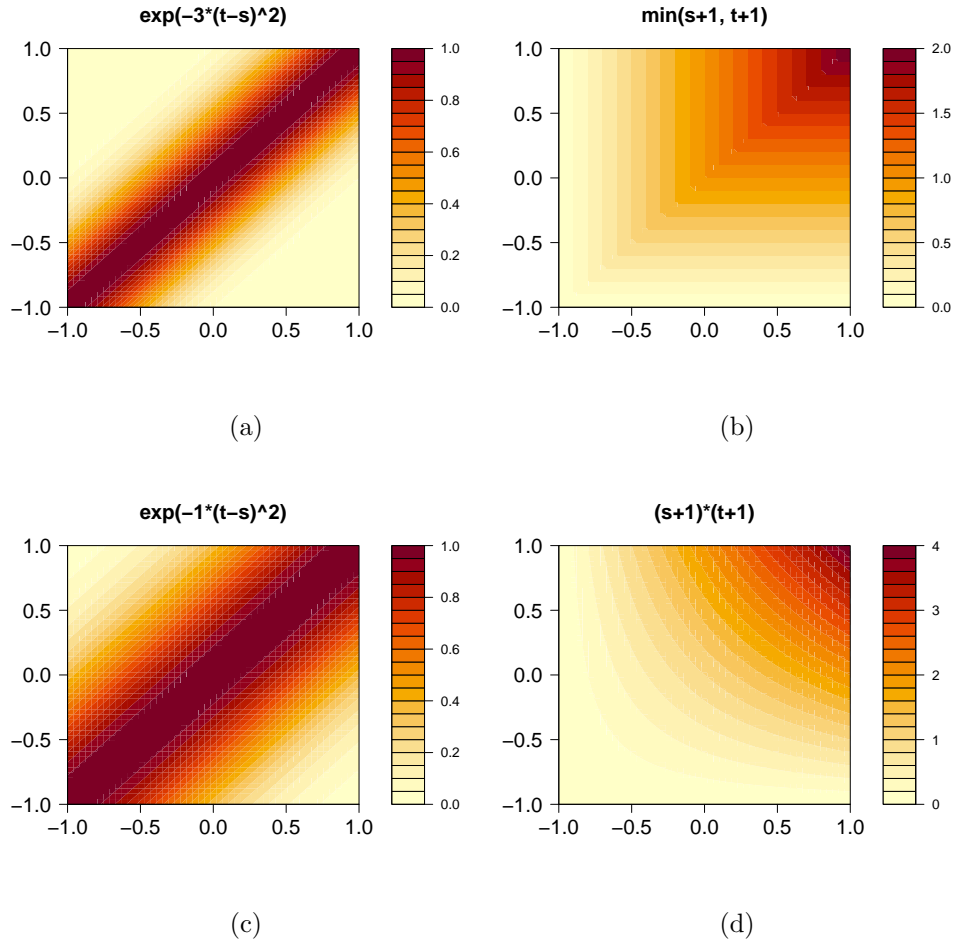


Figure 5: Simulation III: Contour plots of prior covariance functions.

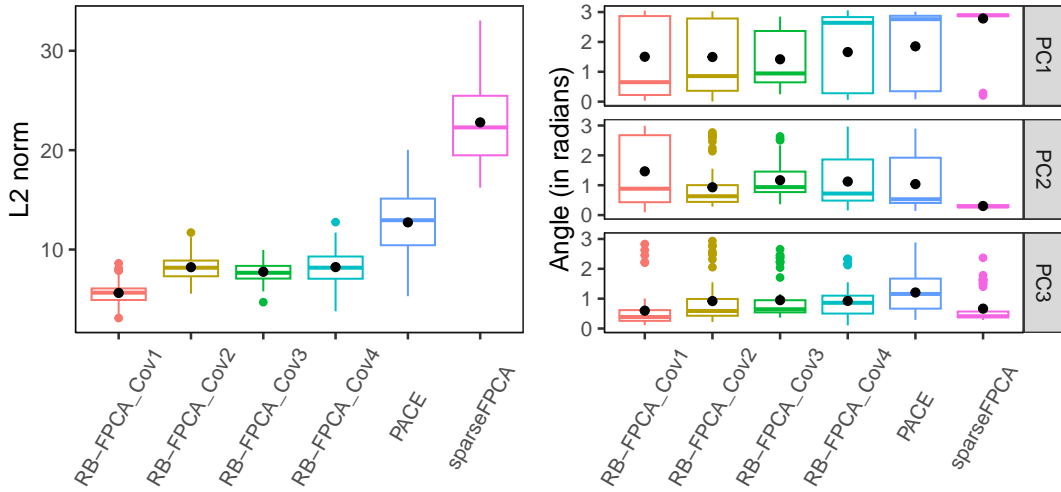
The numbers of basis functions and eigenfunctions are preset as $P = 5$ and $K = 5$. For each setting, a total of 4000 iterations are run, and we discard the first 2000 as the burn-in and use the remainder 2000 for inference. Each setting is repeated 50 times with different seeds and noise levels, and the results are the average of the estimated means from 50 runs. We compared the performance of the proposed RB-FPCA method with two frequentist methods, which are the PACE method of Wang et al. (2016), implemented in `fdapace` package in R, and a robust FPCA (`sparseFPCA`) method of Boente and Salibián-Barrera (2021), implemented in `sparseFPCA` package in R. The performance of each model is compared in terms of estimations of the correlation surface evaluated by L_2 norms and estimations of the first three principal components assessed by the angle (in radians) between

the truth and estimates. Results are presented in Figure 6. Figures 6a and 6b demonstrate the advantage of using the RB-FPCA method over the other two frequentist methods by comparing the estimations of the correlation functions and the PCs. The proposed RB-FPCA method produces better measures of the correlation functions with smaller L_2 norms and admits small variations. Figures 6c and 6d show different methods' performances under the other true covariance function. The proposed RB-FPCA method outperforms one of the frequentist methods, namely sparseFPCA, in terms of the estimations of the correlation functions. PACE performs well for estimating the correlation function, whereas the RB-FPCA method still has a potential advantage if considering the variations of the estimations. Note that even though the sparseFPCA method produces estimations for PCs with the smallest variations, it does not outperform PACE and RB-FPCA methods in estimating the correlation functions and PCs. The robustness of the sparseFPCA method may explain the small variations of the estimations of PCs. The overall picture is that the proposed RB-FPCA method has the ability to deal with sparse longitudinal data, perform competitively with some well-known frequentist methods, and provide a Bayesian framework to enable incorporating the domain knowledge into the analysis via flexible prior settings.

4 Data Applications

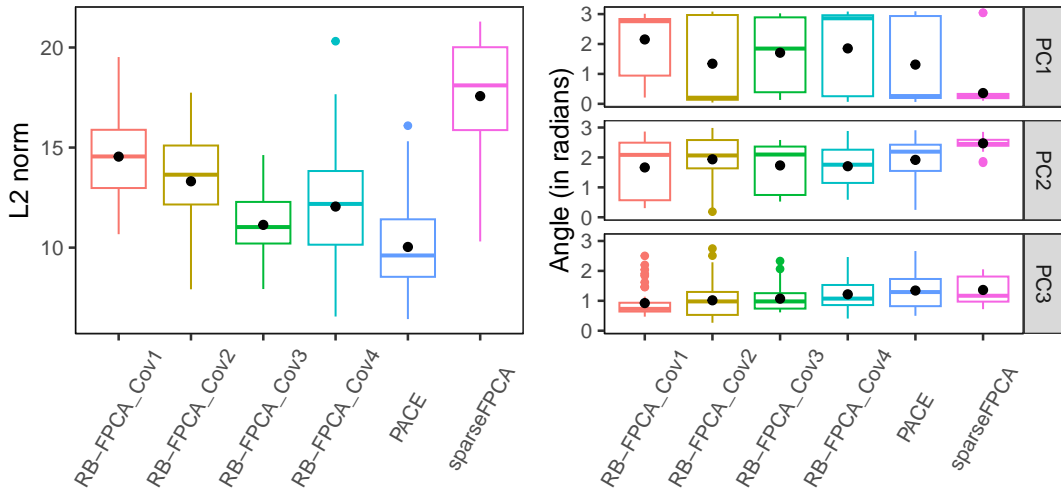
4.1 Hawaii Ocean Oxygen Data

We first illustrate our method on the Hawaii ocean oxygen data collected from the Hawaii Ocean Time-series Data Organization & Graphical System. Scientists participating in the Hawaii Ocean Time-series (HOT) program have been monitoring and making continuous measurements of the water column's hydrography, chemistry and biology at a station near Oahu, Hawaii, since October 1988. The primary objective of this research is to monitor and interpret the variability of physical and biogeochemical processes at deep-water hydrostations and deliver a comprehensive overview of the ocean at a representative site in the North Pacific subtropical region. The deep-water station is visited approximately once



(a)

(b)



(c)

(d)

Figure 6: Simulation III: Comparison of RB-FPCA method with PACE and sparseFPCA methods. (a) and (c) shows boxplots of L_2 norms between the estimates and the true correlation function. (b) and (d) shows boxplots of the angle (in radians) of the estimations for the first 3 principal components. The top row shows the results given the true covariance function is $Cov_{truth}(s, t) = \exp\{-3(t - s)^2\}$. The bottom row shows the results when the true covariance function is $Cov_{truth}(s, t) = \min(s + 1, t + 1)$. The black dots in each box correspond to the values of the mean.

a month by cruises to obtain water samples from desired ocean depths. Observations of ocean data over long periods are extremely valuable for climate studies. Researchers require repeated measurements of oceanographic data to investigate slow or irregular changes in natural processes or phenomena and some rapid event-driven variations. Oceanic data can be downloaded from the Hawaii Ocean Time-series Data Organization & Graphical System website (<https://hahana.soest.hawaii.edu/hot/hot-dogs/cextraction.html>).

In this study, we analyzed the oxygen concentrations in units of $\mu\text{mol}/\text{kg}$ measuring at different depths below the sea surface from January 1, 2008, to December 31, 2021. The oxygen concentration is measured every 2 meters at a depth of 0 to 200 meters under the ocean's surface. Such data with a shorter time frame have been analyzed by Shi and Cao (2022). We obtained 133 trajectories to study the functional relationship between the oxygen concentrations and depth below the sea surface. Each trajectory has 100 data points with no missing values. All trajectories have measurements at the same depths.

We applied the RB-FPCA method for dense data to the Hawaii ocean oxygen data with a predetermined set of numbers of basis functions and eigenfunctions, i.e., $P = 15$ and $K = 5$. The data were first detrended, and the prior covariance function was chosen as $\exp\{-3(t - s)^2\}$. A total of 5000 Gibbs sampling iterations was run, and the first 2500 iterations were discarded as the burn-in. This study aims to find patterns in data of high dimensions, capture the primary mode of variation, and flag potential outliers.

Figure 7 shows the first four FPCs from the RB-FPCA model with variance explained by each FPC. The 95% credible intervals are included with the dashed lines. The credible intervals generated within the Bayesian approach offer a direct interpretation, reflecting the probability of the true parameter being contained within a specific range, for instance, the 95% credible interval indicating a 95% probability of encompassing the true parameter. The credible intervals provide valuable information for interpreting the significance of each FPCs in the analysis. In general, the credible interval for the first FPC is narrow and relatively narrow for the remaining FPCs except at the boundaries. The first FPC is positive and significant over the whole range at a level of 0.05. It represents the weighted average of the oxygen level of each visit to the deep-water station over a depth from 0 to

200 meters. Most of the variation is due to the amount of horizontal shift from the mean function. The second FPC explains about 18% of the total variability. The second FPC can be interpreted as a change in the oxygen level over two depth intervals. The second FPC is positive when the depth is between 0 to 150 meters and negative when the depth is above 150 meters, indicating the relative difference in oxygen levels between 0 to 150 meters and 150 to 200 meters. The credible intervals indicate significant variations over the depth intervals [50, 134] and [152, 200]. FPCs at a higher level represent more complex phenomena. The top 3 FPCs capture over 90 % of the total variation in the data.

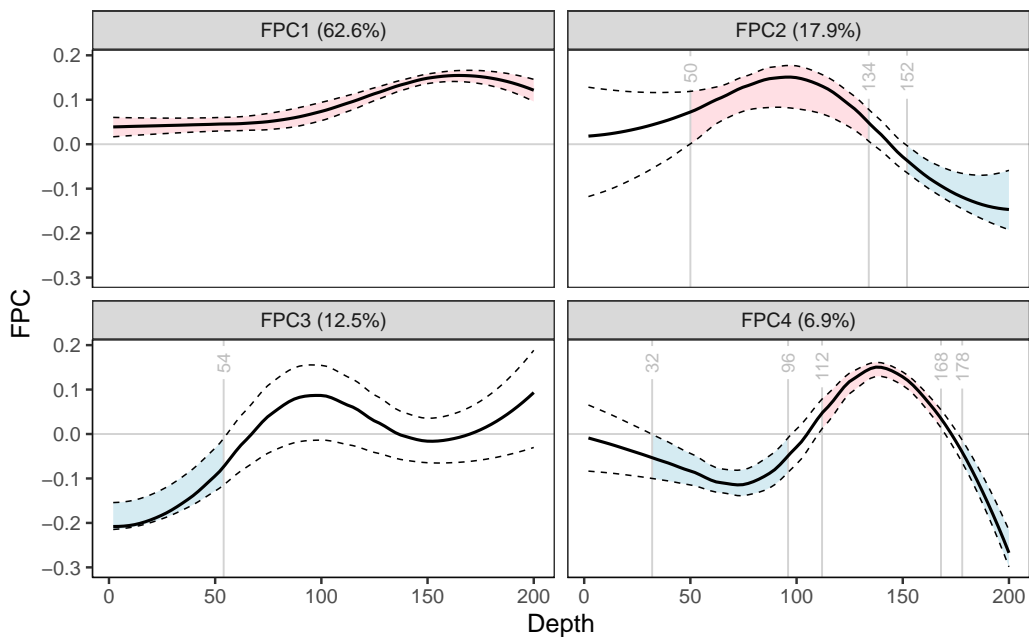


Figure 7: Hawaii Ocean Oxygen Data: The top four estimated FPCs from the full posterior mean of the covariance function with the proportion of variance explained by each FPC. The 95% credible intervals are represented by the dashed lines. The shaded areas denote credible intervals that do not contain zeros. The numeric labels along the vertical lines correspond to the depths associated with the boundaries of each respective shaded area.

We implemented the proposed approach of identifying the outliers using the FPC scores. Different threshold values result in different trajectories being flagged as abnormal. We investigated four threshold values, and the results are presented in Figure 8. The result follows the expectation that fewer outliers are detected as the threshold value increases.

The detected atypical trajectories lie near the top or bottom. Compared with other curves, abnormal trajectories appear to have different curvature, or maintain high values over depth levels, or decline rapidly.

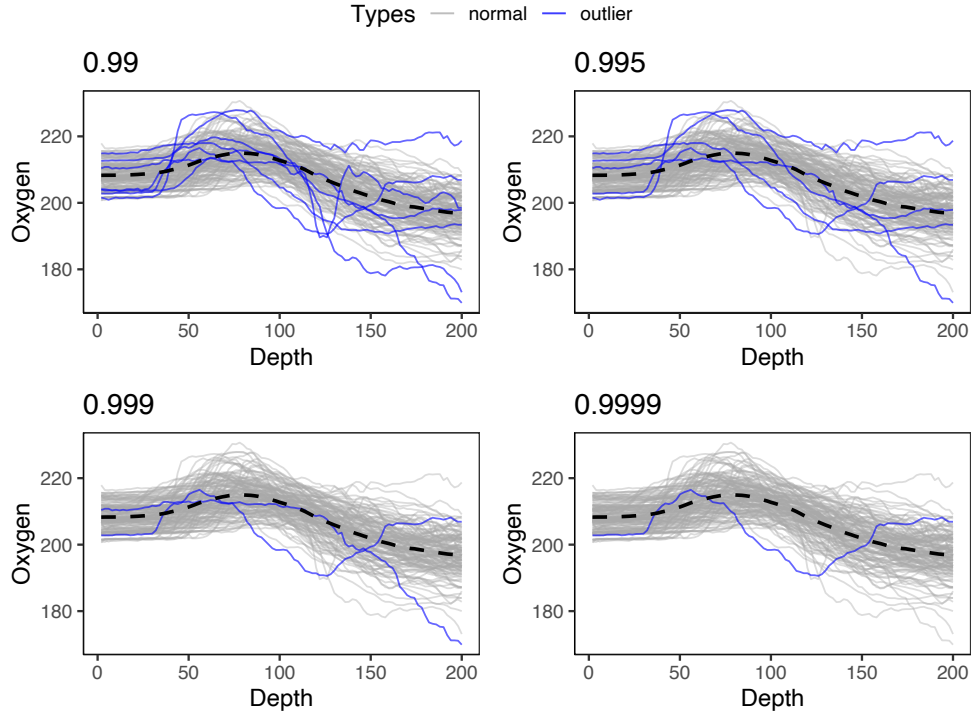


Figure 8: Hawaii Ocean Oxygen Data: Detected outliers and the oxygen trajectories. The dashed curve is the mean function calculated with all trajectories. The values on the top left corner is the threshold value used in the quantile of the χ_2^2 distribution to identify possible outliers. For example, the top left plot shows outliers with FPC scores have distances larger than the 99% quantile of a χ_2^2 distribution.

4.2 Annual sea surface temperature data

The second example considers the annual sea surface temperature data. The sea surface temperature is the temperature of the ocean's surface at its top millimeter. As a fundamental measure of global climate change, sea surface temperature provides a glimpse into the overall trend in the climate system. Understanding the behaviour of the sea surface temperature changes and discovering potential anomalies are essential in studying global

climate change. Sea surface temperature anomalies are characteristic of El Niño and La Niña climate cycles, which can affect weather patterns worldwide. Strong and localized anomalies may identify ocean currents in sea surface temperature. Anomalies in sea surface temperature over many years can be signs of regional or global climate change, for example, global warming. In addition to their scientific value, sea surface temperature anomalies are also useful for practical purposes. For instance, an anomalous temperature (warm or cool) in coastal areas can favor certain organisms in an ecosystem over others, resulting in a thriving or declining population of bacteria, algae, or fish. Such data have been analyzed by Hyndman and Shang (2010), Sun and Genton (2011), Xie et al. (2017), and Dai et al. (2020). Annual sea surface temperature data can be downloaded from the Climate Prediction Center website (<https://www.cpc.ncep.noaa.gov/data/indices/>).

The dataset consists of monthly observations from Niño 1+2 region from January 1950 to December 2021. We obtained 72 functional observations observed on a common grid of 12 time points. They correspond to the monthly sea surface temperature over 72 years. The RB-FPCA method for dense data was applied to find projections of maximum variance. The numbers of basis functions and eigenfunctions are fixed with $P = 10$ and $K = 5$. The prior covariance function that is estimated is $\exp\{-3(t - s)^2\}$. A total of 5000 MCMC iterations were used for estimation after 2500 burn-in iterations. The estimations are only calculated for the time points that have been sampled.

The first two FPCs explain 94% of the variance. The first FPC is almost constant below the zero axis, representing that the major variation is the degree of horizontal shift below the mean function. The second FPC crosses the zero axis once near July, which can be interpreted as the relative change of sea surface temperature between spring and fall months. To investigate the existence of potential outliers, the plot of the FPC scores for the first two FPCs is shown in Figure 9a. We have observed that four observations deviate significantly from the majority of the observations, and have been identified as outliers. The graphical representation of robust Mahalanobis distances in Figure 9b provides further evidence of the outlying behaviors exhibited by these four observations.

From a practical aspect, detecting sea surface temperature anomalies is essential to

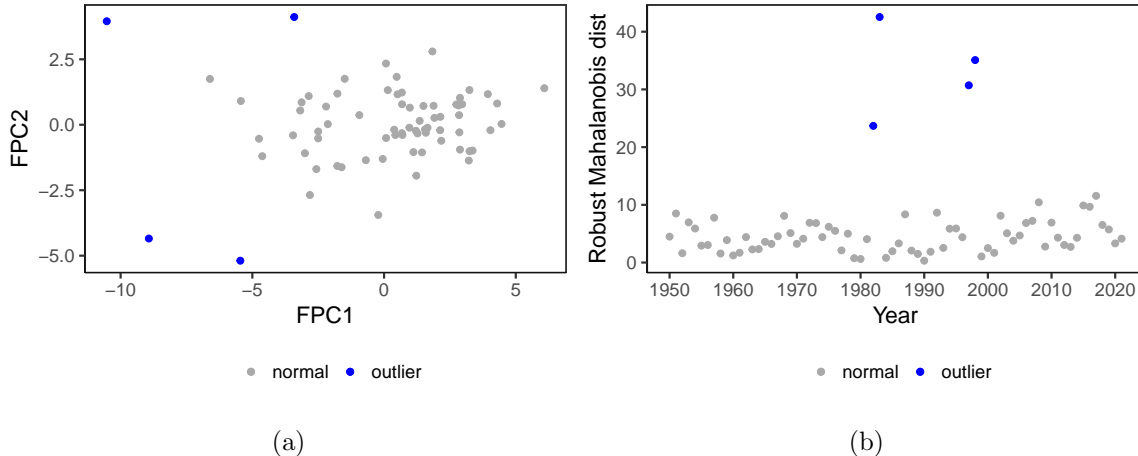


Figure 9: Annual sea surface temperature data: (a) FPC scores for the first two FPCs. Possible outliers and normal observations are differentiated by colors. (b) Plot of the robust Mahalanobis distances for observations. Potential outliers are highlighted. These four suspected outliers correspond to the same observations identified in both (a) and (b).

identify El Niño and La Niña events. El Niño events are widely used to describe the warming of sea surface temperature that occurs every few years. In contrast, La Niña events correspond to years with abnormally low sea surface temperatures. We can determine the abnormal annual sea surface temperature curves by FPC scores with robust Mahalanobis distances larger than 99.5% quantile of a χ_2^2 distribution. Four trajectories (1982, 1983, 1997, and 1998) are identified as anomalies and shown in Figure 10. This finding confirms the potential outliers found from the preliminary investigation of the FPC scores, as depicted in Figure 9. The winters from 1982 to 1983 and 1997 to 1998 have the highest temperatures among all years, and the temperatures remain at high values over the summers of 1983 and 1998. According to National Climatic Data Center reports, these periods correspond to two of the strongest El Niño events in history and are illustrated by squares and triangles in 10a. Although our method cannot flag all significant El Niño or La Niña years, we can detect some of the strongest activities. By decreasing the threshold value in our outlier detection procedure, more outlying curves are expected to appear.

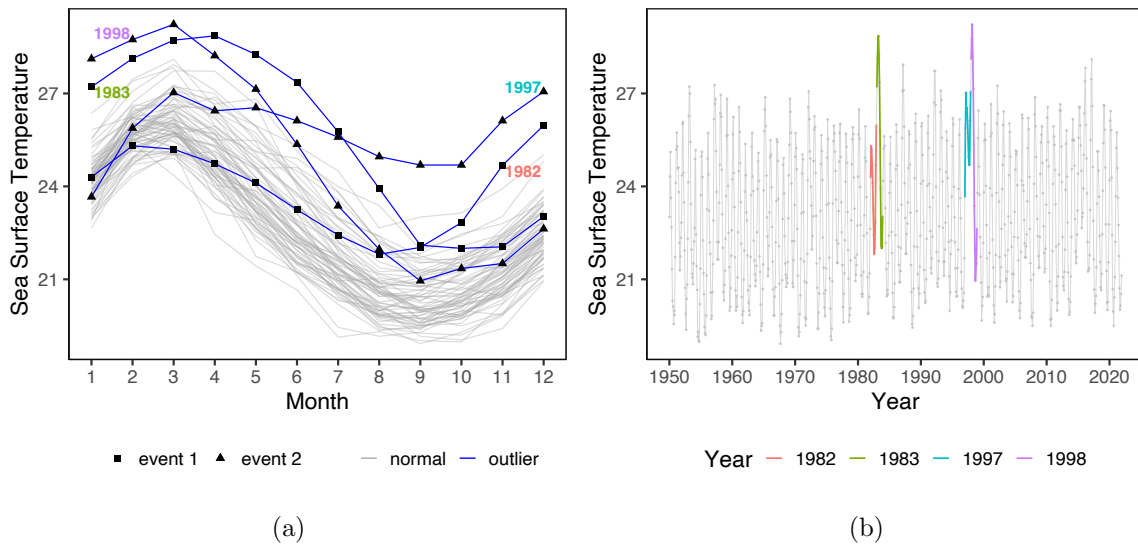


Figure 10: Annual sea surface temperature data: (a) Detected outliers and annual temperature trajectories. The four outliers (blue) are annotated with years, and the colors of the annotations are in line with the legends in panel (b). The detected El Niño events are differentiated by square and triangle. (b) Plot of the whole history of monthly sea surface temperature from January 1950 to December 2021. The locations of the four detected outliers are colored.

4.3 Sparse CD4 Data

The last example considers the CD4 data, a sparse longitudinal dataset collected within the Multicenter AIDS Cohort Study (MACS). Study participants include 1809 HIV-infected men at the start of the study and 371 men who were seronegative at entry and seroconverted during the study period (see Zeger and Diggle (1994)). In our study, we used the data from the `catdata` package in R, which includes 2376 measurements of the number of CD4 cells taken over time on 369 seroconverters. The variable of interest is the CD4 cell counts measured in years since seroconversion, which can be used to assess disease progression. Specifically, we are interested in the typical decay of CD4 cell counts over time and the variability across subjects. The CD4 data are sparse, owing to unequal numbers of repeated measurements for each subject and the different timing of measurements for each subject. We obtained 241 trajectories after removing observations with less than three measurements, and the number of measurements per subject ranges from 3 to 11, with a median of 5. Figure 11a shows the data together with a smooth estimate of the mean function from the PACE method. The overall trend in the CD4 cell counts is decreasing.

We applied the model described in 2.5 to fit the CD4 data and compare the estimates of the covariance function with the PACE method. We used a fixed number of basis functions and eigenfunctions, i.e., $P = 3$ and $K = 3$, and ran a total of 5000 Gibbs sampling iterations with 2500 burn-in iterations. We utilized the PACE method's estimates of the covariance function as the prior covariance function because such an informative prior expresses one's beliefs about this quantity. The tuning parameters for the PACE method were set to default values as described in Wang et al. (2016).

We identified some potential outliers using the estimated FPC scores from conditional expectations. The top five most outlying trajectories are identified and highlighted in Figure 11b. These outlying trajectories appear to have either some rapid decreases or increases compared to the rest. They also tend to have overall CD4 cell counts very high compared to the others during the whole period. We estimated the covariance functions using all the trajectories and only normal trajectories. The comparisons of the covariance function estimates under RB-FPCA and PACE are displayed in Figure 12. The RB-FPCA

and PACE estimators have similar overall shapes, whereas RB-FPCA produces a more smooth surface. When outliers are removed, RB-FPCA induces a similar covariance surface compared with the estimation from complete data except near the boundary, demonstrating the robustness of the RB-FPCA model.

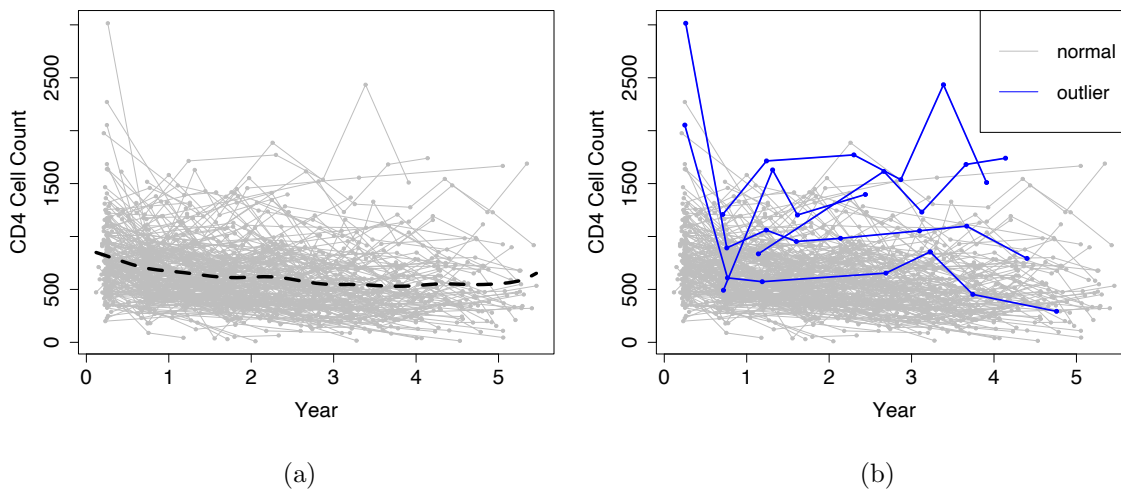
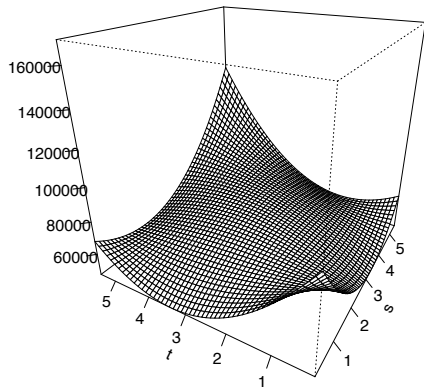


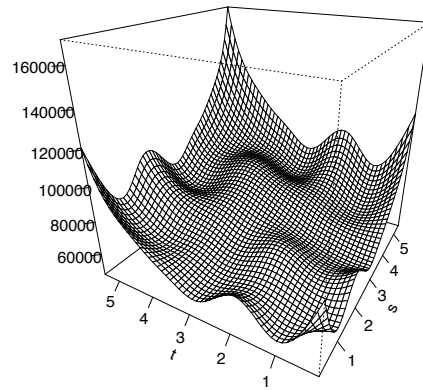
Figure 11: Sparse CD4 Data: (a) Data contain 241 observed trajectories for CD4 cell counts. The dashed line is the smooth estimate of the mean function. (b) Detected five most outlying trajectories in CD4 data.

5 Discussion

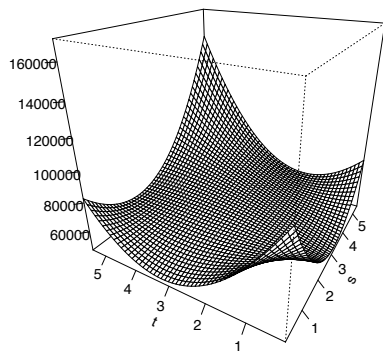
In this work, we developed a robust Bayesian functional principal components analysis method that utilizes the class of skew elliptical distributions in the modelling. The general and flexible class of skew elliptical distributions can serve as an alternative to the symmetric distribution commonly assumed in the previous works of Bayesian FPCA. The proposed method is able to handle the sparse longitudinal data in which only a few observations per trajectory (possibly sampled at irregular intervals) are available. Such data are commonly seen and attracted interest in the area of functional data analysis. We have shown in simulation studies and data applications that the proposed method can effectively capture



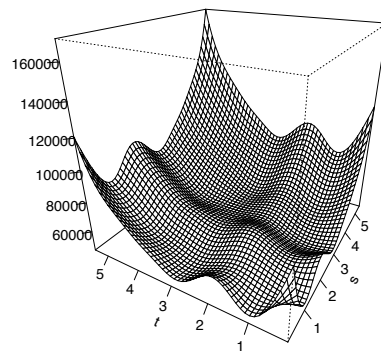
(a) RB-FPCA (complete data)



(b) PACE (complete data)



(c) RB-PFCA (outliers removed)



(d) PACE (outliers removed)

Figure 12: Sparse CD4 Data: Comparison of smooth estimates of the covariance functions under RB-FPCA and PACE. The covariance surfaces are estimated with all trajectories in (a) and (b) and with the five most outlying trajectories removed in (c) and (d).

the major variation and provide useful information in the presence of noises and outliers in the data.

Multiple future directions of research are presented as follows. The class of skew elliptical distribution contains many standard families of distributions such as the multivariate skew normal distribution, Student- t and Pearson type II distributions. We have only presented the case of multivariate skew normal distribution in this work, and multivariate skew- t distribution is another particular example which has the ability to deal with heavier-tailed data. Extending the current framework to fit the multivariate skew- t distribution is straightforward by modifying some equations presented in 2.2. Specifically, we introduce n i.i.d random variables w_i , and the hierarchical representation of the model with multivariate skew- t distribution for $i = 1, \dots, n$ is

$$\begin{aligned} \mathbf{Y}_i | \cdot &\sim MVN_T(\mathbf{H}_P \mathbf{U}_K \boldsymbol{\beta}_{i,K} + \mathbf{D} \mathbf{z}_i, \boldsymbol{\Sigma}/w_i), \\ w_i &\sim \text{Gamma}(\nu_{w_i}/2, \nu_{w_i}/2), \\ \nu_{w_i} &\sim \text{Gamma}(1, 0.1)I(\nu_{w_i} > 2). \end{aligned}$$

The other distributional specifications remain the same. For the specifications of the full conditional distributions, the only part that depends on w_i is for \mathbf{z}_i in equation 11 where $\mathbf{A}_i = \mathbf{I} + w_i \mathbf{D} \boldsymbol{\Sigma}^{-1} \mathbf{D}$ and $\mathbf{a}_i = w_i \mathbf{D} \boldsymbol{\Sigma}^{-1} (\mathbf{Y}_i - \mathbf{H}_P \mathbf{U}_K \boldsymbol{\beta}_{i,K})$. Implementing the multivariate skew- t distribution could improve the model performance, which requires further exploration.

Furthermore, the standard FPCA operates in a static way, therefore, does not provide an adequate dimension reduction when considering the functional time series data. Hörmann et al. (2015) proposed a dynamic FPCA which takes into account the serial dependence in the functional time series. A Bayesian version of the robust FPCA for functional time series is worth investigating. Regarding posterior inference, there exist popular alternative algorithms, such as reversible jump Markov Chain Monte Carlo or sequential Monte Carlo, which could provide some advantages in computation and model selection. Further research into the computational aspects of the robust Bayesian FPCA methods is necessary.

SUPPLEMENTARY MATERIAL

R code for RB-FPCA R code implements the proposed model described in the article.

All datasets used as examples in the article are also included.

References

- Azzalini, A. and A. D. Valle (1996). The multivariate skew-normal distribution. *Biometrika* 83(4), 715–726.
- Behseta, S., R. E. Kass, and G. L. Wallstrom (2005). Hierarchical models for assessing variability among functions. *Biometrika* 92(2), 419–434.
- Boente, G. and M. Salibián-Barrera (2021). Robust functional principal components for sparse longitudinal data. *METRON* 79(2), 159–188.
- Branco, M. D. and D. K. Dey (2001). A general class of multivariate skew-elliptical distributions. *Journal of Multivariate Analysis* 79(1), 99–113.
- Cardot, H. (2000). Nonparametric estimation of smoothed principal components analysis of sampled noisy functions. *Journal of Nonparametric Statistics* 12(4), 503–538.
- Chib, S. (1995). Marginal likelihood from the Gibbs output. *Journal of the American Statistical Association* 90(432), 1313–1321.
- Crainiceanu, C. M. and A. J. Goldsmith (2010). Bayesian functional data analysis using WinBUGS. *Journal of Statistical Software* 32, 1–33.
- Dai, W., T. Mrkvička, Y. Sun, and M. G. Genton (2020). Functional outlier detection and taxonomy by sequential transformations. *Computational Statistics & Data Analysis* 149, 106960.
- Dauxois, J., A. Pousse, and Y. Romain (1982). Asymptotic theory for the principal component analysis of a vector random function: some applications to statistical inference. *Journal of Multivariate Analysis* 12(1), 136–154.

- Ferraty, F. and P. Vieu (2006). *Nonparametric Functional Data Analysis*. New York: Springer.
- Fukunaga, K. and W. L. Koontz (1970). Representation of random processes using the finite Karhunen-Loeve expansion. *Information and Control* 16(1), 85–101.
- Hall, P. and M. Hosseini-Nasab (2006). On properties of functional principal components analysis. *Journal of the Royal Statistical Society: Series B (Statistical Methodology)* 68(1), 109–126.
- Han, C. and B. P. Carlin (2001). Markov chain Monte Carlo methods for computing Bayes factors: A comparative review. *Journal of the American Statistical Association* 96(455), 1122–1132.
- Hörmann, S., Ł. Kidziński, and M. Hallin (2015). Dynamic functional principal components. *Journal of the Royal Statistical Society: Series B (Statistical Methodology)* 77(2), 319–348.
- Horváth, L. and P. Kokoszka (2012). *Inference for Functional Data with Applications*. New York: Springer.
- Hsing, T. and R. Eubank (2015). *Theoretical Foundations of Functional Data Analysis, with an Introduction to Linear Operators*. Chichester: John Wiley & Sons.
- Hyndman, R. J. and H. L. Shang (2010). Rainbow plots, bagplots, and boxplots for functional data. *Journal of Computational and Graphical Statistics* 19(1), 29–45.
- James, G. M., T. J. Hastie, and C. A. Sugar (2000). Principal component models for sparse functional data. *Biometrika* 87(3), 587–602.
- Jeffreys, H. (1935). Some tests of significance, treated by the theory of probability. In *Mathematical Proceedings of the Cambridge Philosophical Society*, Volume 31, pp. 203–222. Cambridge University Press.

- Jiang, L., Y. Zhong, C. Elrod, L. Natarajan, R. Knight, and W. K. Thompson (2020). BayesTime: Bayesian functional principal components for sparse longitudinal data. *ArXiv Preprint ArXiv:2012.00579*.
- Jolliffe, I. T. (2002). *Principal component analysis for special types of data*. Springer.
- Margaritella, N., V. Inácio, and R. King (2021). Parameter clustering in Bayesian functional principal component analysis of neuroscientific data. *Statistics in Medicine* 40(1), 167–184.
- Paul, D. and J. Peng (2009). Consistency of restricted maximum likelihood estimators of principal components. *The Annals of Statistics* 37(3), 1229–1271.
- Ramsay, J. and B. Silverman (2005a). Principal components analysis for functional data. pp. 147–172.
- Ramsay, J. O. and B. W. Silverman (2005b). *Functional Data Analysis* (Second ed.). New York: Springer.
- Rasmussen, C. E. (2003). Gaussian processes in machine learning. In *Summer School on Machine Learning*, pp. 63–71. Springer.
- Reiss, P. T., J. Goldsmith, H. L. Shang, and R. T. Ogden (2017). Methods for scalar-on-function regression. *International Statistical Review* 85(2), 228–249.
- Rice, J. A. and B. W. Silverman (1991). Estimating the mean and covariance structure nonparametrically when the data are curves. *Journal of the Royal Statistical Society: Series B (Methodological)* 53(1), 233–243.
- Sahu, S. K., D. K. Dey, and M. D. Branco (2003). A new class of multivariate skew distributions with applications to Bayesian regression models. *Canadian Journal of Statistics* 31(2), 129–150.
- Shi, H. and J. Cao (2022). Robust functional principal component analysis based on a new regression framework. *Journal of Agricultural, Biological and Environmental Statistics*, 1–21.

- Suarez, A. J. and S. Ghosal (2017). Bayesian estimation of principal components for functional data. *Bayesian Analysis* 12(2), 311–333.
- Sun, Y. and M. G. Genton (2011). Functional boxplots. *Journal of Computational and Graphical Statistics* 20(2), 316–334.
- Uhlig, H. (1994). On singular Wishart and singular multivariate Beta distributions. *The Annals of Statistics*, 395–405.
- Van Der Linde, A. (2008). Variational Bayesian functional PCA. *Computational Statistics & Data Analysis* 53(2), 517–533.
- Wang, J.-L., J.-M. Chiou, and H.-G. Müller (2016). Functional data analysis. *Annual Review of Statistics and Its Application* 3, 257–295.
- Xiao, L., V. Zipunnikov, D. Ruppert, and C. Crainiceanu (2016). Fast covariance estimation for high-dimensional functional data. *Statistics and Computing* 26(1), 409–421.
- Xie, W., S. Kurtek, K. Bharath, and Y. Sun (2017). A geometric approach to visualization of variability in functional data. *Journal of the American Statistical Association* 112(519), 979–993.
- Yao, F., H.-G. Müller, and J.-L. Wang (2005). Functional data analysis for sparse longitudinal data. *Journal of the American Statistical Association* 100(470), 577–590.
- Yohai, V. J. (1987). High breakdown-point and high efficiency robust estimates for regression. *The Annals of statistics*, 642–656.
- Zeger, S. L. and P. J. Diggle (1994). Semiparametric models for longitudinal data with application to CD4 cell numbers in HIV seroconverters. *Biometrics*, 689–699.